Agricultural and Forest Meteorology 237 (2017) 160–170

Contents lists available at ScienceDirect

Agricultural and Forest Meteorology

journal homepage: www.elsevier.com/locate/agrformet

Combining eddy-covariance and chamber measurements to determine the methane budget from a small, heterogeneous urban floodplain wetland park

T.H. Morin[a,*], G. Bohrer[a], K.C. Stefanik[a,b], A.C. Rey-Sanchez[a], A.M. Matheny[a], W.J. Mitsch[b,c]

[a] Department of Civil and Environmental Engineering and Geodetic Science, The Ohio State University, Columbus, OH, USA
[b] School of Environment and Natural Resources, The Ohio State University, Columbus, OH, USA
[c] Everglades Wetland Research Park, Florida Gulf Coast University, Naples, FL, USA

ARTICLE INFO

Article history:
Received 30 March 2016
Received in revised form 16 January 2017
Accepted 29 January 2017

Keywords:
CH4
Land-surface heterogeneity
Surface-atmosphere interactions
Eddy covariance
footprint model
Olentangy River Wetland Research Park

ABSTRACT

Methane (CH_4) emissions and carbon uptake in temperate freshwater wetlands act in opposing directions in the context of global radiative forcing. Large uncertainties exist for the rates of CH_4 emissions making it difficult to determine the extent that CH_4 emissions counteract the carbon sequestration of wetlands. Urban temperate wetlands are typically small and feature highly heterogeneous land cover, posing an additional challenge to determining their CH_4 budget.

The data analysis approach we introduce here combines two different CH_4 flux measurement techniques to overcome scale and heterogeneity problems and determine the overall CH_4 budget of a small, heterogeneous, urban wetland landscape. Temporally intermittent point measurements from non-steady-state chambers provided information about patch-level heterogeneity of fluxes, while continuous, high temporal resolution flux measurements using the eddy-covariance (EC) technique provided information about the temporal dynamics of the fluxes. Patch-level scaling parameterization was developed from the chamber data to scale eddy covariance data to a 'fixed-frame', which corrects for variability in the spatial coverage of the eddy covariance observation footprint at any single point in time. By combining two measurement techniques at different scales, we addressed shortcomings of both techniques with respect to heterogeneous wetland sites.

We determined that fluxes observed by the two methods are statistically similar in magnitude when brought to the same temporal and spatial scale. We also found that open-water and macrophyte-covered areas of the wetland followed similar phenological cycles and emitted nearly equivalent levels of CH_4 for much of the year. However, vegetated wetland areas regularly exhibited a stronger late-summer emission peak, possibly due to CH_4 transport through mature vegetation vascular systems. Normalizing the eddy covariance data to a fixed-frame allowed us to determine the seasonal CH_4 budget of each patch and the overall site. Overall, the macrophyte areas had the largest CH_4 fluxes followed by the open water areas.

Uncertainties in the final CH_4 budget included spatial heterogeneity of CH_4 fluxes, the tower footprint, measurement in the data to be scaled, and gap-filling. Of these, the spatial placement of the chambers provided the largest source of uncertainty in CH_4 estimates. This reinforces the need to utilize site-level measurements when estimating CH_4 fluxes from wetlands as opposed to using only up-scaled point measurements.

1. Introduction

In the late 1980′s, the United States government set a goal of 'no net loss' of wetlands to preserve their ecological services. The net result has been the creation of new or the restoration of existing wetlands to mitigate the destruction or damage of natural wetlands due to human activities (US-EPA, 2012). Required mitigation activities are determined by quantifying the ecological services provided by the natural wetland. To date, structural hydrogeomorphic and biological indicators are employed to estimate functional ecosystem services (Mack et al., 2004). The overall climatological effects of wetlands are not yet well understood, and therefore are not

* Corresponding author at: 470 Hitchcock Hall, 2070 Neil Avenue, Columbus, OH 43210, USA.
E-mail address: morin.37@osu.edu (T.H. Morin).

http://dx.doi.org/10.1016/j.agrformet.2017.01.022
0168-1923/

currently considered when determining the qualities of replacement wetlands. Wetlands are strong sinks of carbon dioxide (CO_2) (Hommeltenberg et al., 2014a; Mitsch et al., 2013, 2014; Schäfer et al., 2014; Waletzko and Mitsch, 2013). However, wetlands are also the largest natural source of methane (CH_4) worldwide (IPCC, 2013), and are a powerful source of nitrous oxide (N_2O), another strong greenhouse gas (GHG). The balance of these GHGs determines the net climatological effect of a wetland. In part, the lack of climatological understanding stems from the larger uncertainty in the global wetland CH_4 budget (IPCC, 2013). Traditionally, the quantification of CH_4 emissions from wetlands has been difficult for several reasons. Perhaps chief among these is the heterogeneity of land cover in wetlands and the relatively small scale at which the different patch types are distributed (on the order of meters). This is further complicated by the interactions between biotic and abiotic ecosystem components that govern CH_4 production and transport within each patch.

Currently, the foremost techniques for measuring CH_4 emissions are the eddy covariance (EC) and the closed chamber methods. The eddy covariance method observes turbulent GHG fluxes (Baldocchi et al., 1988) for monitoring trace gas flux dynamics at a landscape level. Eddy covariance towers have become a common approach for monitoring CH_4 emissions from temperate wetlands (Baldocchi et al., 2012; Forbrich et al., 2011; Hatala et al., 2012a,b; Hommeltenberg et al., 2014a,b; Long et al., 2010; Morin et al., 2014a; Wang et al., 2013). High-frequency EC measurements are collected continuously, capturing diurnal and seasonal dynamics. However, the sensors atop EC towers observe CH_4 dynamics from a constantly shifting footprint area (Hsieh et al., 2000; Kljun et al., 2015). The location and size of the surface area that contributes to fluxes observed at the tower top (at a certain height above and downwind from the sources) is determined by wind speed, wind direction, friction velocity, and surface heat flux (among other factors) (Detto et al., 2006). This is rarely a concern for EC towers placed in homogenous terrain as all source terrain is assumed to have uniform fluxes. However, in heterogeneous environments, or when EC measurements are conducted from tall towers or airborne platforms, which result in a very large footprint, a footprint-weighted approach for downscaling flux measurements to the patch level was previously demonstrated for environmental fluxes of CO_2 and energy (Hutjes et al., 2010; Maurer et al., 2013; Metzger et al., 2013; Ogunjemiyo et al., 2003; Wang et al., 2006). Similarly, footprint-weighted approaches were utilized to downscale patch-level model results or chamber measurements in order to compare them with instantaneous EC measurements (Budishchev et al., 2014; Frasson et al., 2015).

Wetlands are frequently composed of a tight mosaic of land cover types (often referred to as microsites or patch types), such as open water, obligate and facultative wetland plant species (macrophytes), grasslands, dry land (uplands), and temporarily flooded (bottomland) forests. Furthermore, the length scale of homogeneity in wetlands is short, and the CH_4 fluxes associated with each patch type can differ by orders of magnitude (Nahlik and Mitsch, 2010; Sha et al., 2011). In heterogeneous landscapes with strong patch-level variability in flux rates, the apparent temporal dynamics of the observed flux may, therefore, not only be driven by changes in the emission rates, but also by the movement of the footprint area from one patch type to another. Understanding how fluxes vary between and among patch types is critical to understanding the total CH_4 budget of the wetland ecosystem.

The CH_4 emission rates from specific components of heterogeneous terrain can be directly measured using the non-steady state chamber method. Multiple chambers can be used to measure various patch types in an area, and thus, chamber data can be used to illustrate differences in flux magnitude between patches. Chambers are broadly grouped as either manual chambers (requiring a technician to draw samples) or automated chambers (automatically sample at regular time intervals). Both classes of chambers have potential drawbacks. Manual chamber measurements are labor intensive, which greatly limits the total number of chambers that can be sampled. Automated chamber measurements rely on closed-path gas analyzers that need to be placed in close proximity to the chambers, and are relatively expensive. Automated chambers are therefore limited in the spatial distance between chambers and the number of patches they can sample. Because of these limitations, manual chamber studies are more common. In most cases, manual chamber data are gathered during the day on an intermittent sampling schedule, typically on a monthly or biweekly basis. As a result, sudden, high magnitude flux events and diurnal dynamics are rarely observed via chamber techniques (Morin et al., 2014b; Podgrajsek et al., 2014). Additionally, chamber measurements are often filtered to remove ebullition (Altor and Mitsch, 2006; Bellisario et al., 1999; Christensen et al., 2003; Leppala et al., 2011) and are ineffective when turbulent diffusion is the dominant transport mechanism due to the disruption of wind over shallow water (Godwin et al., 2013). In many studies, chamber data for methane fluxes have been up-scaled to the site level (Clement et al., 1995; Desai et al., 2015; Godwin et al., 2013; Podgrajsek et al., 2014; Schrier-Uijl et al., 2010). However, point measurements cannot effectively sample the full spatial variation of patch-specific fluxes from the wetland landscape. Similarly, they cannot observe the full short-term (intra-daily) and intermediate (inter-daily) temporal variations that occur within a site. As a result, several studies have shown that up-scaling temporally and spatially sparse point measurements can bias site-level flux estimates (Desai et al., 2015; Forbrich et al., 2011; Sachs et al., 2008; Zhang et al., 2012).

The limitations of flux monitoring techniques have restricted the quality of wetland CH_4 flux estimates. Combining chamber point observations with eddy covariance site-level observations has the potential to mitigate the weaknesses associated with using either method on its own. Forbrich et al. (2011) and Sachs et al. (2010) successfully combined the two methods to down-scale eddy covariance data in sites with regularly patterned terrain (northern polygonal peatlands). However, little work has focused on unpatterned and varied terrain, as is typical of mid-latitude wetland ecosystems (Matthes et al., 2014).

In this study, we used eddy covariance and chamber measurements of CH_4 in tandem to correct for their respective limitations and achieve a better estimate of the patch-level and overall site-level net CH_4 budget. A continuous time series of CH_4 emissions from a 'fixed-frame' area comprised of the different patch types was established at the urban wetland park. The fixed-frame approach normalized the flux levels to a non-shifting site level footprint with the particular mixture of patch types of interest to the study. Chamber measurements were used to correct for the effects of patch-type emission variability within the footprint of the eddy covariance tower. We then conducted an uncertainty analysis of the final scaled CH_4 data product to determine the contributions of different sources of uncertainty to the overall fixed-frame flux estimate.

2. Methods

2.1. Site description

The study was conducted at the Wilma H. Schiermeier Olentangy River Wetland Research Park (ORWRP), a 20 ha research facility located on the Ohio State University campus in Columbus, Ohio. The site was designed in 1991-92 with the initial experimental wetlands constructed in 1993–94. The ORWRP consists of two 1 ha created experimental flow-through wetlands, a 3 ha created oxbow wetland, a restored 7 ha bottomland hardwood forest, 3 small ornamental wetlands, and the Olentangy River, a 3rd-order stream that serves as the main source of water for the wetlands. Vegetation cover in the experimental wetlands included *Juncus effusus*, *Acorus calamus*, and *Typha* spp. (*Typha latifolia*, *Typha angustifolia*, and *Typha* x *glauca*).

In addition to the aquatic ecosystems, the site also contains the Heffner Wetland Research Building, a small managed lawn around the building, unmanaged grasslands, and short-canopy upland forests emerging between and around the wetland ecosystems. For the purposes of this study, the park was broadly separated into 4 patch types: 1) open water, 2) vegetated (macrophyte), 3) seasonally flooded oxbow wetland, and 4) bottomland hardwood forest/managed.

The emerging bottomland forest adjacent to the experimental wetlands is approximately 10 m tall and is still growing. The average summer air temperature is 21.3 (°C) while average winter temperature is 5.0 °C. The pH of the experimental wetland is 7.7, and the average soil carbon content is 3.6 kgC m^{-2} (Bernal and Mitsch, 2013).

2.2. Eddy covariance measurements

The EC flux data used for this study are available through the Ameriflux network, site ID US-ORv. Eddy covariance data has been collected continuously at the site since April 2011. The flux calculation approach for the site is fully outlined in Morin et al. (2014b). In brief, a 3D rotation was applied to wind observations to force the vertical and cross wind components to average to 0 for each half-hour (Lee et al., 2004). To correct for the separation of the sensors, the time series of concentration measurements were shifted in time using the maximal-covariance approach (Detto et al., 2011). CO_2 (net ecosystem exchange, *NEE*), CH_4, and water vapor flux (latent heat flux, *LE*) were corrected according to Webb, Pearman, and Leuning (WPL) (1980) to account for the effects of changes in the densities of dry air and water vapor. Frequency response corrections for *LE* and CH_4 fluxes, which are based on concentration measurements from open-path gas analyzers (LI-COR Bioscience, LI-7500 for water vapor and CO_2, and LI-7700 for CH_4) were calculated using the approach of Massman (2000), as validated by Detto et al. (2011). CH_4's absorbance spectrum is temperature dependent. We therefore combined an absorbance spectrum correction with the WPL correction as detailed in the LI-7700 manual (LI-COR, 2010). Day-night transition was calculated using PAR or shortwave radiation observations night was defined as when the radiation variable dropped below 10 W/m^2. For the purpose of gap-filling techniques and footprint calculations that are dependent on the surface roughness parameters (and thus leaf phenology), we assume a 2-season annual cycle. Transition dates between summer and winter were determined through the carbon flux phenology approach (Garrity et al., 2011). According to this approach, the growing season is when the 2 week moving average of net ecosystem exchange of CO2 flux is negative and the dormant season is defined as when the moving average of NEE is positive.

The standard empirical approach of defining a seasonal threshold value of friction velocity (u^*) that indicates an insufficient level of turbulent mixing was used to reject invalid data (Reichstein et al., 2005). The u^* and carbon flux data were first separated into six temperature classes. Within each temperature class, the u^* and carbon flux were further separated into 20 classes based on u^*. The u* class in which the mean carbon flux was at least 95% of the mean carbon flux from all higher u^* classes was selected. The overall u^* threshold was taken as the median u^* cutoff value over all six temperature classes. The minimum value allowed for a u^* threshold was 0.2 m/s in the summer and 0.15 m/s in the winter. The u^* filter was used for both carbon and methane fluxes on the assumption that if the turbulence is sufficient to provide adequate mixing conditions for carbon flux measurements it will be sufficient to do the same for methane.

The height of the tower was altered three times over the life of the study; once in April 2012 (9 m–15 m) to compensate for forest growth, once in October 2013 (15 m–12 m) to keep the sample footprint within the park during the winter when surface roughness is low and conditions are more often stable, and once in April 2014 (12 m–15 m) to return the tower to growing-season height.

Eddy covariance flux data was gap-filled after applying the fixed-frame correction according to Morin et al. (2014b) using the automated neural network (ANN) approach, an expanded version of the method commonly used in flux sites, introduced by Papale and Valentini (Moffat et al., 2007; Morin et al., 2014b; Papale and Valentini, 2003; Reichstein et al., 2005). Gap-filling is necessary as eddy covariance data are more commonly discarded at night and in the winter by the u^* filtering process, which may lead to biased estimates if not gap-filled properly. We first divided the data set into summer and winter periods to be gap-filled separately. CH_4 gap-filling variables for summer were the latent heat flux, footprint percentage of the experimental wetlands, soil temperature, u^*, air temperature, and NEE. The winter gap-fill variables were latent heat flux, sensible heat flux, NEE, u^*, relative humidity, footprint percentage of the experimental wetlands, soil temperature, and water vapor concentration. All gap-filling driver variables were determined in Morin et al. (2014a) experimentally. The neural network first normalizes all predictor variables between 0 and 1 then uses combinations of these variables to minimize the error of the modeled flux. The architecture for our neural network used a hyperbolic tangent sigmoid (tansig) transfer function to produce 12 hidden nodes from the input predictor variables. These hidden nodes were then entered into another tansig transfer function to produce a new set of five hidden nodes. These five nodes were then passed through a final tansig transfer function to produce the output layer. The model uses a random 50% of the data as the training period for parameterization; another non-overlapping 25% of the data for validation of the parameter estimate and the remaining data are used to evaluate the overall model performance (i.e., calculate r^2). Only valid data are considered for training, validation, and evaluation. The neural network creates up to 100 models using a particular training set. If the model created on the training set exceeded a minimum r^2 value (initially set to 0.75) on the testing data set, the model was accepted as one possibility. Each possible model created based on the training set was then evaluated against the testing set. Only if the r^2 on the testing set was sufficiently high did we continue with a particular model. The minimum r^2 value was reduced to the average testing set $r^2 + 0.1$ if after 5000 attempts to model the flux no sufficient model was created. This process continued until a sufficiently high scoring model was created, at which point a single iteration of the ANN had completed. We created 1000 ANN iteration models for each flux variable and then selected the best 10% of those models (determined by the r^2 of the model of the complete set) and averaged the results from this ensemble of 100 modeled ANNs to create our final model. The standard deviation of this ensemble was used as an estimate of the uncertainty of the model and observations.

2.3. Eddy covariance footprint model

A footprint model was used to determine the probability of origin locations for concentrations and fluxes during each 30 min aggregated flux measurement. We used the footprint model to quantify the relative contribution of each microsite to the observed site-level flux observation during a particular half hour. The model is a multi-patch expansion of the 2-D model by Detto et al. (2006), which is based on the 1-D model by Hsieh et al. (2000).

The footprint model used gap-filled wind speed, wind direction, roughness length, displacement height, boundary layer stability, and turbulence observations to trace the probability that a parcel of air measured at the flux-tower top originated from any particular point in the wetland park.

$$z_u = (z_H - D)\left(\ln\left(\frac{z_H - D}{z_0}\right) - 1 + \frac{z_0}{z_H - D}\right) \quad (1)$$

$$F = \frac{1}{k^2x^2}P_1 \cdot {z_u}^{P_2}|L|^{1-P_2}{z_u}^{P_2}e^{\frac{1}{k^2x}P_1{z_u}^{P_2}|L|^{1-P_2}} \quad (2)$$

where z_u is a characteristic length scale, z_H is the measurement height, D is the displacement height, z_0 is the roughness length, F is the footprint contribution along the primary wind direction, k is the von Karman constant (0.4), x is a range of distances from the tower along the primary wind direction, L is the Obukhov length, and P_1 and P_2 are similarity constants with different values for stable, unstable, and neutral atmospheric conditions. The standard deviation of the crosswind footprint was determined according to Detto et al. (2006).

$$\sigma_y = a_1 z_0 \frac{\sigma_v}{u*}\left(\frac{x}{z_0}\right)^{p_3} \quad (3)$$

where a_1 and P_3 are similarity constants with values of 0.3 and 0.86 respectively and σ_v is the crosswind variation ($v'v'$) of each half hour as measured by the sonic anemometer.

The model generated a 'tear-drop' shaped footprint area for each half hour measured. This footprint area was defined so that there is a 90% probability that the observed flux originated from that area. The infinite tail of the probability distribution (accounting for the remaining 10%) was truncated. The footprint shape was oriented to the primary wind direction for the half hour and was then superimposed on a pixel map of the site where each pixel was given a code corresponding to its patch type. We integrated the partial contribution of each patch type within the footprint area and considered the patch-type integral to be representative of the relative contribution of that patch. It is important to note that all current generation EC footprint models are designed for homogeneously rough terrains. In this study, some level of error due to roughness transitions between the water surface, wetland vegetation, and forested upland is implicitly accepted through its use. The magnitude of this error is difficult to estimate. Large eddy simulations (LES) could provide a reasonable approximation for a short time period. However, since LES could not feasibly be run over seasons (with current computational power even days-long simulations are difficult) a traditional footprint model was used to quantify the season-long flux origin.

2.4. Non-steady state chambers

Closed system, non-steady state chambers have been used to collect GHG samples from the two experimental wetlands since 2003 to examine various research questions (Altor and Mitsch, 2006, 2008; Nahlik and Mitsch, 2010; Sha et al., 2011; Waletzko and Mitsch, 2014). For this study, a total of eight open water, eight macrophyte, and two upland (area under forest) sites were sampled per month from April to September/October in 2011 and 2012 and from January to March in 2013. In 2014, four open water sites and two macrophyte areas were sampled per month from June through October. Floating chambers (0.056 m^3) were used to collect samples from open water areas, while collared chambers (0.1 m^3) were used to collect samples from vegetated and upland sampling locations.

Samples were collected from each chamber using a vial and syringe method. 30 mL gas samples were collected from a sampling port on the closed chambers using a syringe every 5 min over a 30-min time frame. The first sample was collected as soon as the chamber was put into place (time zero) and was representative of atmospheric conditions. The 30 mL samples were stored in 10 mL glass vials that had been evacuated using a vacuum pump (Gast Manufacturing Inc., Model 0523-V4-6588DX) prior to sampling. Samples were run on a Shimadzu GC-2014 gas chromatograph equipped with a Flame Ionization Detector (FID) that measures CH_4, and a methanizer that converts CO_2 to CH_4 for analysis by the FID. The gas chromatograph was calibrated prior to running each month's samples. A four point calibration curve was created for methane at concentrations of 5, 10, 15, and 20 ppm using calibration grade gas standards of methane and nitrogen as the dilution gas (Matheson Tri-Gas Micro Mat 14 Methane 100 ppm, GMT10341TC, and Matheson Tri-Gas Micro Mat 14 Nitrogen 99.998% min, GMT10020TC). Methane check standards at 5, 10, 15, and 20 ppm were run with sample batches to ensure the gas chromatograph maintained its calibration throughout analysis.

Laboratory analysis of the chamber samples was performed as described in Altor and Mitsch (2006). Concentrations were corrected for air density in field conditions using a modified Ideal Gas Law from Holland et al. (1999):

$$C_m = \frac{C_v \cdot M \cdot P}{R \cdot T} \quad (4)$$

where C_m is the mass/volume concentration of the gas (i.e. mg CH_4-C m^{-3}), C_v is the volume (ppm) of gas, M is the molecular weight of element of interest, P is atmospheric pressure (atm), R is the universal gas constant (0.0820575 L atm K^{-1} mol^{-1}), and T is the air temperature (K) of the chamber.

The accumulation rate was determined using the slope of the linear regression fitted to the time points collected for each chamber. Flux was calculated using the equation from Holland et al. (1999):

$$f = \frac{v \cdot C_{rate}}{A} \quad (5)$$

where f is the flux rate (mg CH_4-C m^{-2} h^{-1}), V is volume of chamber (m^3), C_{rate} is the accumulation rate in mg CH_4-C m^{-3} h^{-1}, and A is area of soil surface (m^2).

2.4.1. Comparing up-scaled chamber and uncorrected EC flux observations

We up-scaled chambers to the eddy covariance level to verify that the measurements were reasonably near one another. A simpler approach of upscaling chambers to EC observations of CO_2 fluxes is a single patch type demonstrated by Lavigne et al. (1997) and Ohkubo et al. (2007). Here, we conducted the upscaling in order to validate each set of measurements and to ensure that ample chamber sampling had been done to characterize the site properly. To do this, we averaged chamber measurements per patch type and integrated to the site level by multiplying the observed mean flux for each patch type by the average contribution of that patch type to the observation footprint of eddy covariance measurements during the time period the chamber measurements were conducted. In addition to spatial adjustments, temporal corrections are also needed when comparing intermittent samples with continuous ones. Chamber measurements from different times (chamber data was collected from different locations over the course of 1-3 days) were temporally corrected by multiplying them by the ratio between eddy covariance measurements gathered within two hours of the measurement and the full daily average of eddy covariance measurements within the 4 day averaging period.

2.4.2. Scaling from variable-footprint to fixed-frame fluxes

Scaling equations were developed by combining eddy covariance and non-steady state chamber observations to obtain a 'fixed-frame' flux time series representing the flux of CH_4 from spatially integrated experimental wetland area at any given point in time. The ORWRP was first broadly classified into four patch types for CH_4 emissions: 1) open water (ow), 2) macrophyte (veg), 3) upland (ul −managed lawn and forest ground cover), and 4) oxbow (ox). Each eddy covariance measurement is therefore a mixture of the specific fluxes from these patch types, each with their respective fractional contribution to the measurement footprint.

$$F_{obs} = e_{ow}F_{ow} + e_{veg}F_{veg} + e_{ul}F_{ul} + e_{ox}F_{ox} \quad (6)$$

where F_{obs} is the CH_4 flux observed by the eddy covariance tower, F marks the flux from each patch type (indicated by a subscript other than '*obs*') and e (of different patch types, indicated by subscript) is the fraction of the eddy covariance measurement footprint that originates from each of the patch types.

Unlike the flux-observation footprint, the permanently flooded area of the wetland site does not vary every half hour and, for a given year, is composed solely of open water and macrophytes.

$$F_{site} = f_{ow}F_{ow} + f_{veg}F_{veg} \quad (7)$$

where F_{site} is the actual overall flux of the experimental wetlands (i.e. the desired 'fixed-frame' value) and f_{ow} and f_{veg} are the area coverage fractions of the experimental wetlands open water and vegetated patch types, respectively. We allowed f_{ow} and f_{veg} to vary annually, representing the interannual variability of the vegetated-patch area. Annual field campaigns were carried out throughout the course of the study to determine the area of the experimental wetlands covered by open water and vegetation. From 2011–2013, this was accomplished through a manual field campaign using a GPS unit to map vegetation and open water areas of the wetlands. We matched these ground-based observations to aerial images of the wetland obtained through the Ohio Department of Natural Resources. In 2014, the vegetation layout was mapped out relative to the boardwalk by measuring the distance and direction of the vegetation to the boardwalk at several points. Data from the GPS unit and aerial images were mapped and rasterized using QGIS to calculate the percentage cover of vegetation and open water for each year (Quantum, 2013).

Site-level fluxes may be approximated from direct chamber measurements using Eq. (7). However, studies have found it is more effective to down-scale eddy covariance data than to up-scale chamber data owing to chamber measurements' exclusion of turbulent diffusion, the difficulties representing all possible patch types (Forbrich et al., 2011; Sachs et al., 2008), and the limited temporal coverage of the chamber observations (Morin et al., 2014b). In this study, chamber observations were used to constrain the unknown patch-level flux terms (F) in Eq. (6). As the oxbow fluxes were not measured with chambers during this study, we used the mean value obtained in previous years in our site by Sha et al. (2011), 0.09 mgCH$_4$-C m^{-2} s^{-1}, for F_{ox} when the oxbow area is flooded and 0 when the oxbow is dry as CH_4 production and flux is dependent on water levels (Altor and Mitsch, 2006; Bohn et al., 2007; Leppala et al., 2011; Moore and Dalva, 1993). F_{UL} was assumed to be negligible (0 mgCH$_4$-C m^{-2} s^{-1}) if no chamber measurement was available, as our observations and others in the site indicate that it fluctuates around zero and does not have a significant impact on the overall site level flux dynamics (Sha et al., 2011).

We assume that during a particular month, corresponding with monthly chamber measurements, F_{ow} and F_{veg} are related, as the two originate from similar soil types and are affected by the same above-wetland meteorological forcing. We assume a scalar relationship between the two at any point in time as no hypothesis supported a more complex relationship.

$$F_{veg} = mF_{ow} \quad (8)$$

where the ratio variable, m, is allowed to vary with time. As with any other footprint-weighted analysis approach, we assume that the flux rates within a given patch type and a single observation period (here, half hour) are fixed. Additionally, we assume that consistent heterogeneity in flux rates exist between but not within patch types. Therefore, for a given half-hour measurement period, the entire wetland is represented by a single m value. We make the assumption that the flux rates within the two permanently flooded patch types are related. We do so because the two patches have similar soil characteristics, are in very close proximity, and are driven by identical meteorological forcing. This relationship, along with the estimates for F_{ul} and F_{ox} were used to solve Eq. (6) for open water, providing F'_{ow} and F'_{veg}which are the estimated flux from these patch types (open water, and macrophyte-covered wetland, respectively) as determined from the eddy-covariance time series (F_{obs}) combined with the relative strength of the flux between these patch types (m) as determined by the chamber measurements.

$$F'_{ow} = \frac{F_{obs} - e_{ul}F_{ul} - e_{ox}F_{ox}}{e_{ow} + e_{veg}m}$$
$$F'_{veg} = \frac{F_{obs} - e_{ul}F_{ul} - e_{ox}F_{ox}}{e_{veg} + \dfrac{e_{ow}}{m}} \quad (9)$$

It is important to note that the estimated F'_{ow} and $F'_{veg}$are different (and potentially more representative of reality) than those measured by the chambers as they were derived from the continuous EC measurements, thereby capturing the temporal dynamics of mature vegetation, turbulent diffusion, and ebullition. These approximated values are then used with Eq. (7) to give an estimate of the site-level fluxes over the fixed area of the permanently flooded component of the site:

$$F_{site} = f_{ow}F'_{ow} + f_{veg}F'_{veg} \quad (10)$$

2.5. Uncertainty of scaled fluxes

As an unavoidable outcome of the assumptions in our analysis and the limited accuracy of the measurement techniques, the results of our analysis are associated with some range of uncertainty. An uncertainty analysis was used to determine 4 potentially large sources of error in the final scaled product: 1) gap-filling error, 2) chamber measurement uncertainty, 3) uncertainty due to spatial placement of the observation (i.e., assuming a spatially fixed m value), and 4) footprint uncertainty. We also analyzed the propagation of chamber measurement error and spatial error through the gap-filling process.

Gap-filling uncertainty was estimated as the mean squared error of the neural network. The neural network uses a portion of the target data for training and the rest for evaluation and validation. Mean squared error is found by using the neural network model to recreate the full CH_4 flux data set (including points where observations exist) and comparing the modeled fluxes to the observed. Gap-filling uncertainty only occurs at points where observations were missing.

In chambers, a single measurement is derived from the slope of a regression model fit over the multiple replicate sampled concentration values for the measurement period. The slope is an estimate of the accumulation rate that is then used to determine the flux (Eq. (5)). Chamber measurement uncertainty was estimated by estimating the error in the regression of CH_4 concentration accumulation data used to generate each chamber flux measurements.

$$s_b = \left[\sum\left(y_i - \hat{y}_i\right)^2\right]^{0.5} \times \left[(n-2)\sum\left(x_i - \bar{x}\right)^2\right]^{-0.5} \quad (11)$$

where s_b is the error of the slope in the regression, y_i is the CH_4 concentration measurement value within a given chamber at time i, $\hat{y}_i$ is the regression-predicted CH_4 concentration for the same time, n

is the number of concentration observation samples within a single chamber measurement, x is the time of observation (minutes), and $\bar{x}$ is the mean time of the observations. We used the observed mean flux value and added a Gaussian signal with a standard deviation equal to the mean error of all chamber measurements for the same patch type during the same month as a characteristic estimate for the distribution of potential chamber flux values. We then sampled 800 simulated random potential chamber-flux values for each patch type based on the uncertainty and mean of each month. We subsampled sets of 8 random 'measurements', simulating the actual number of chambers in the observation campaign, to create 100 unique possible realizations of both open water and vegetation chambers at every measurement period. These were paired randomly and the ratio between them gave us 100 possible realizations of the variable m (used in Eq. (8)) based on the measurement uncertainty. These m values were used to generate iterations of possible fixed-frame CH_4 fluxes. The mean squared error between these iterations and the original estimate was taken as the measurement uncertainty. To simulate the compounding of measurement error through the gap-filling process, we utilized the scaling equations with each of the iterations then used the neural network to gap-fill each 100 times, for a total of 10,000 runs to characterize the full effect of the measurement error. The mean squared error of this was calculated and describes the superposition of measurement and gap-filling uncertainty.

A similar process was used to estimate the uncertainty due to the spatial placement of the chambers. A modified version of V-CaGe (Bohrer et al., 2007), a numerical generator of random spatially-autocorrelated fields, was used to simulate a distribution of emission values per patch type in the ORWRP. We determined the autocorrelation functions that describe the spatial distribution of methane fluxes. This was achieved by grouping chamber measurements into sets based on the observation location. This allowed us to estimate the correlation of fluxes between two locations as a function of separation distance. We fit a negative exponential distribution to these data and used the fit as the autocorrelation function. A separate autocorrelation function was estimated for each patch type. V-CaGe then used a random phase matrix and the autocorrelation function to create a map of potential flux values where points with similar flux magnitudes were spatially grouped. We generated such 'flux fields' per patch type. Each patch-type specific field was scaled using the mean and standard deviation of the patch flux levels which were observed from the chambers. Finally, we superimposed the fields of different patch types using the actual patch location in the physical map of the site (e.g. Fig. 1). These flux maps were simulated with V-CaGe for every month in which we had chamber data. This gave us a theoretical set of maps with flux values at every location that was classified according to each patch type. Similar to measurement uncertainty, we simulated 800 random chamber locations per patch type for each month, and again aggregated them in sets of 8 into 100 possible observations per month. These were again paired for 100 m values and used in the scaling equation for 100 iterations of the F_{site} time series. This allowed us to examine what the effects of sampling at any possible combination of 8 locations throughout the wetlands would have had on the end result of estimated total methane fluxes. We used the mean squared error among this ensemble of random locations compared to the observation-based estimate to determine the effect of spatial placement of the chamber observations. To represent the superposition of spatial uncertainty and gap-filling uncertainty, we used the neural network 100 times for each representation of F_{site} and found the average mean squared error of these iterations.

Footprint uncertainty was estimated by gap-filling the daily CH_4 flux time series according to Morin et al. (2014a). The variables used in this study were the same as those found to have the greatest influence in that manuscript; however, any variables that could

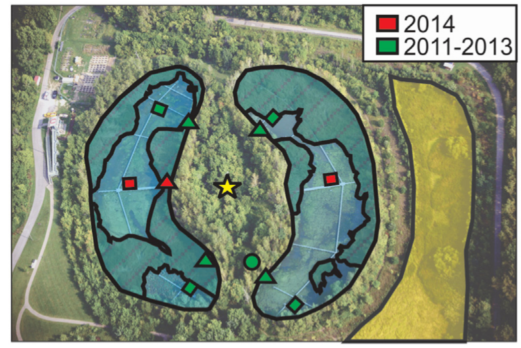

Fig. 1. The Olentangy River Wetland Research Park and CH_4 flux sampling locations. Squares show the location for open water chambers, triangles for macrophyte chambers, and the circle for the upland chambers (colors indicate the time period of sampling as indicated in the legend). The yellow star shows the eddy-covariance tower location. The shades represent the land-cover types, where the green hatched area is macrophyte vegetation, light blue is open water, and yellow is the temporarily flooded oxbow. The exact location of the vegetation changes from year to year and this image presents the patch types at 2012. The unshaded portions are covered by forest, managed lawn, or impervious surface (roads, parking lots), which we assume do not contribute to the methane budget of the site. (For interpretation of the references to colour in this figure legend, the reader is referred to the web version of this article.)

contain footprint information were excluded from the process to determine a baseline error. This includes wind direction, *NEE*, and the footprint itself. We took the relative difference between the goodness of fit of the ANN without footprint-related variables and the goodness of fit of the best ANN determined by Morin et al. (2014a), with footprint added, as an estimate for the potential size of the error that could be attributed to the footprint. This methodology bounded the error that could be attributable to footprint error, but the exact uncertainty of footprint models in heterogeneous environments is not easily quantified. The bounding methodology only yielded significant results in the summer when the footprint is generally smaller and therefore, more dependent on the exact extent of the footprint. In the winter, the footprints are typically very large and include most of the site, and thus, while incorporating much larger uncertainty overall, the methane estimates are less dependent on the accuracy of the footprint estimate.

3. Results and discussion

3.1. Up-scaling chambers to the site level

By combining the relative flux intensities as observed by chamber measurements and the relative contribution of each patch type to the EC footprint, we used Equation (10) to scale the fluxes from each patch type to the corresponding eddy flux observations. When properly scaled, CH_4 chamber measurements closely matched the eddy covariance tower observations (Fig. 2). Different approaches to process-based bottom-up scaling have been tested before (Desai et al., 2015; Forbrich et al., 2011; Metzger et al., 2013; Parmentier et al., 2011). Our results suggest that tower footprint heterogeneity can be corrected for through adequate supplementary measurements. This opens up sampling and interpretation in a larger host of wetlands than would be available through traditional flux processing.

This agreement also indicates that the chamber sampling was performed at adequate spatial and temporal scales to consistently converge on the eddy covariance tower measurements over several seasons and years (Savage and Davidson, 2003; Sha et al., 2011; Sturtevant and Oechel, 2013). The chambers typically indicated higher flux levels than the eddy covariance tower in the summer months, but lower levels in the winter months (Fig. 2).

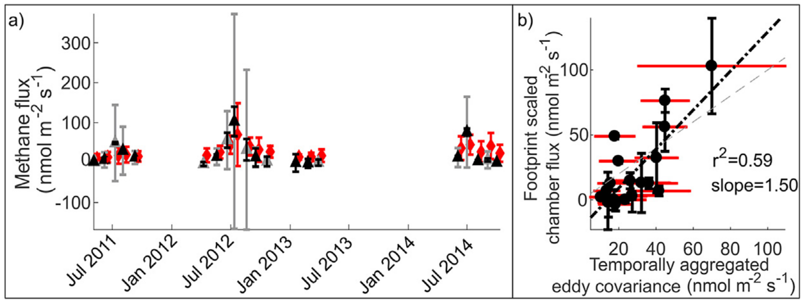

Fig. 2. a) Chamber observations scaled to eddy covariance observations. Black triangles mark chamber measurements. Red diamonds indicate eddy covariance measurements averaged for two days before to two days after the chamber measurements were collected. Black error bars for the chambers represent the mean measurement error associated with the chambers. The larger grey error bars give the standard deviation of measurements among chambers aggregated to the site level. This roughly represents the spatial variability of CH_4 fluxes throughout the wetland, indicating that the heterogeneity of fluxes even within a given patch type can result in large uncertainties in wetlands. The red error bars for the EC flux represent the standard deviation of half-hourly EC fluxes within 2 day averaging period. b) Regression of chambers upscaled to the tower footprint level with temporally aggregated eddy covariance. Vertical and horizontal error bars indicate the uncertainty associated with chamber (only measurement uncertainty) and EC measurements, respectively. A grey dashed line marks the 1:1 relationship. A bold dashed line marks the regression model between the two. The two data sets agree well with one another ($r^2 = 0.59$, slope = 1.50) The scaled chambers tend to underrepresent low fluxes and overestimate high flux levels. (For interpretation of the references to colour in this figure legend, the reader is referred to the web version of this article.)

Some disagreement is to be expected, and other scaling studies have similarly found that up-scaled chamber measurements do not adequately represent the site level (Forbrich et al., 2011; Hendriks et al., 2010; Sachs et al., 2008; Yu et al., 2013). The fluxes observed by the two approaches were usually within one standard deviation of each other and were almost never significantly different (Fig. 2). These generally small differences may indeed be due to the spatial distribution of fluxes within patch types. Measurements were always taken in deep portions of the wetland, which are likely to have higher fluxes within the same patch type than the fluxes from shallower areas during the summer (Blodau and Moore, 2003; Brown et al., 2014; Goodrich et al., 2015; Moore et al., 2011). Similarly, in the winter, large portions of CH_4 are emitted by bubbles through cracks in the ice, which would not be measured by the chambers but would be captured by the EC tower (Rinne et al., 2007).

The majority of flux scaling studies have been 'upscaling studies' such as done here and conducted for CO_2 (Lavigne et al., 1997; Ohkubo et al., 2007; Wang et al., 2006) as well as CH_4 fluxes (Budishchev et al., 2014; Forbrich et al., 2011; Sachs et al., 2010; Schrier-Uijl et al., 2010; Zhang et al., 2012). Interpretation of airborne and tall tower observations adopt similar assumptions and footprint-weighted approach for disaggregation of whole-footprint EC observations to the patch level (Budishchev et al., 2014; Desai et al., 2015; Hutjes et al., 2010; Metzger et al., 2013; Ogunjemiyo et al., 2003).

3.2. Methane budget of the site

Eddy covariance data was filtered by the u^* filter, footprint filter, and despiking process as shown in Table 1. The u* filter almost always eliminated the most data (with the exception of winter 2012–2013 when the footprint was prohibitively large).

Contributions to the CH_4 budget by patch type are shown in Table 2. The macrophyte patch type was the greatest emitter of CH_4 throughout the park on both a per unit area basis as well as an aggregated total for the park. Open water also emitted a significant amount of CH_4. We hypothesize that the addition of labile carbon to the soil in the macrophyte patch increased the amount of CH_4 that could be synthesized. This is consistent with findings by Christensen et al. (2003) and Whiting and Chanton (1993) who showed that the addition of accessible microbial substrate by plants leads to higher methane fluxes. The lawn and forest ground cover were observed to be a slight sink for CH_4 in this study (assumed to be of the same magnitude). More complex interactions may be taking place at the leaf or stem level throughout the forest canopy but these were not targeted for study (but see Grosse et al., 1996; Kim et al., 1999; Kutzbach et al., 2004; Stefanik and Mitsch, 2014; Terazawa et al., 2007; Whiting and Chanton, 1996). These dynamics have been shown to have an influence on site level methane budgets of wetlands seasonally and should be an effort for future studies (Kim et al., 1999; von Fischer et al., 2010). The oxbow had very low effective CH_4 fluxes, most likely due to the flood/drying cycle within that patch type (Sha et al., 2011). Overall, the dry areas surrounding the experimental wetlands served as a CH_4 sink but did not offset the emissions from the permanently flooded portions of the park, making the park as a whole a net source for CH_4.

3.3. Corrected fixed-frame methane fluxes

The ratio between the open water and macrophyte fluxes showed a strong phenological trend (Fig. 3). While changing diurnal dynamics of fluxes from wetland area covered with *Typha* spp. have been observed in other studies (Kim et al., 1999; Whiting and Chanton, 1996), the data gathered in this study were not sufficient to quantify the dynamics and so the temporal dynamics of patches were only accounted for based on daytime CH_4 flux activity. Due

Table 1
Data filtering of eddy covariance data.

	Season length Days	Data available Days	Eliminated by u* Days	Eliminated by footprint Days	Despiked Days	Data remaining Days
Summer 2011	164	79.04	37.1	0	0.19	41.75
Winter 2011–2012	189	124.15	24.5	0	1.15	98.5
Summer 2012	175	112.48	38.52	32.15	0.35	41.46
Winter 2012–2013	207	156.73	28.17	114.13	0.35	14.08
Summer 2013	162	128.56	37.63	24.75	0.4	65.79
Winter 2013–2014	206	123	16.23	0.27	1.96	104.54
Summer 2014	152	84.17	32.85	0.31	0.27	50.73

Table 2
Overall CH_4 budget in the site. The upper panel shows the budget broken down by patch type using the scaling methodology developed in this study. Error shown is one standard deviation. η – (Sha et al., 2011). The bottom portion of the table shows the site flux by year calculated three ways 1) Directly upscaling chambers to the eddy covariance footprint level, 2) Using traditional eddy covariance processing, and 3) Using the fixed-frame processing developed here. Traditional EC measurements, which intrinsically assume homogeneous land cover, have the largest discrepancy from what is believed to be the true site level fluxes. Upscaled chambers and the fixed-frame processing give similar values but the uncertainty is greatly reduced through the incorporation of eddy covariance data. Years with relatively low wetland coverage had the greatest change between their fixed-frame and traditional EC estimates.

	Open Water	Plant	Forest	Oxbow	Lawn
Coverage m^2	6734–9543	10457–13266	165115	30000	22240
CH_4 gC m^{-2} yr^{-1}	47.5 ± 9.0	59.6 ± 10.4	−3.6 ± 1.6	0.7 ± 0.4η	−3.6 ± 1.6

	Site Level Flux			Footprint			
	Upscaled Chams MgC yr^{-1}	Traditional EC MgC yr^{-1}	Fixed-Frame (flooded patches) MgC yr^{-1}	Open Water %	Plant %	Upland %	Oxbow %
2011	2.23 ± 2.33	0.15 ± 0.04	1.36 ± 0.1	3.23	8.94	6.84	1.04
2012	1.18 ± 1.28	0.21 ± 0.04	1.18 ± 0.07	6.26	13.13	13.67	4.22
2013	1.04 ± 1.12	0.18 ± 0.04	0.91 ± 0.07	7.79	11.98	13.91	5.02
2014	0.52 ± 0.31	0.22 ± 0.04	0.99 ± 0.08	9.77	16.2	15.48	4.08
Total	1.20 ± 1.23	0.19 ± 0.04	1.09 ± 0.08	6.88	12.64	12.79	3.79

to the low magnitude of fluxes during the winter months, the ratio between fluxes from both patch types (m) is highly sensitive to small observation variations during this season and its values display unusual spikes in the early summer of 2011. Typically, during most of the year, the two fluxes are similar and the ratio wavers about 1, only deviating strongly during the end of the growing season (Fig. 3). The late summer peak of vegetated area fluxes indicates that the plant activity best supports CH_4 production at certain times in the year causing it to become the dominant emitter (Kim et al., 1999; Whiting and Chanton, 1993). Wetland methane emissions are known to be highly dependent on plant communities (Joabsson et al., 1999; Kim et al., 1999; Mikkelä et al., 1995; Wilson et al., 1989). Similar to Kim et al. (1999) and Ström et al. (2005), we find that the developmental stage of wetland vegetation played a major role in the seasonal cycle of methane fluxes.

The relationship between open water and macrophyte CH_4 flux levels from chamber measurements was used to determine the fixed-frame overall fluxes from the site (Eq. (9)). When scaling the eddy covariance observations from the flux footprint to the fixed-frame of the actual area of the experimental wetlands, the overall site-level fluxes were within the range of CH_4 fluxes at other sites (Baldocchi et al., 2012; Hatala et al., 2012b; Li and Mitsch, 2016). Other recent eddy covariance studies have shown consistent methane fluxes (as opposed to different by an order of magnitude, as is the case with uncorrected fluxes here) between years, further supporting this correction

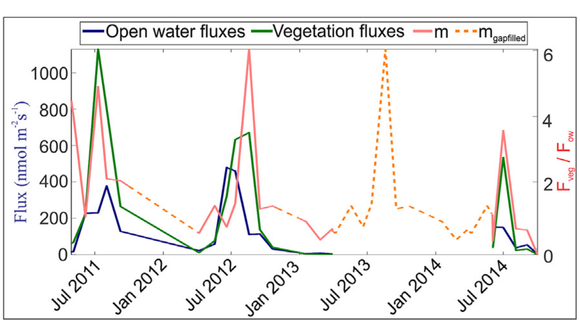

Fig. 3. "Cool" colors show the measured flux levels as observed by chambers (left axis): Open water (blue) and macrophyte (green). Both follow similar phenological trends but the macrophyte patch tends to have a stronger peak. The ratio of the open water to macrophyte patch fluxes is shown in "warm" colors (right axis): Observed ratio (red) and gap-filled (orange). For most of the year the ratio is nearly 1, but during late summer the macrophyte flux is significantly higher than the open water fluxes. (For interpretation of the references to colour in this figure legend, the reader is referred to the web version of this article.)

(e.g. Fortuniak et al., 2017; Jackowicz-Korczyński et al., 2010; Wille et al., 2008). A direct example for the effectiveness of scaling the fluxes to a fixed-frame is apparent by comparing the fluxes for 2011 and 2012. In 2011, the EC tower was lower (at 10 m) and the footprint typically had a higher upland contribution originating from the forested patch that surrounds the tower between the two experimental wetlands (see Fig. 1). This resulted in low magnitude CH_4 fluxes measured by the tower. In 2012, after the tower height was raised (to 12 m) and the overall wetland fraction within the footprint increased, the observed fluxes were considerably higher (note the difference between 2011 and 2012 in Fig. 2, and in Morin et al., 2014b, Fig. 4). However, when accounting for the flux from the fixed-frame area of the permanently flooded component of the wetland park, the magnitude of the 2011 fluxes became much closer to that observed in 2012 (Table 2). Additionally, scaling the eddy covariance data to the fixed-frame level brought the budget close to that given when chambers were directly up-scaled. In addition to hypothetical improvement of measurements through this scaling approach, the uncertainty of the fixed-frame approach was considerably lower than that of simply upscaling the chambers directly.

3.4. Uncertainty in scaled fluxes

Overall uncertainty of the fluxes was highest in the summer, and propagation through the neural network predictably increased both spatially and with measurement uncertainty (Fig. 5). When observations existed and were not gap-filled, measurement uncertainty played only a small role of the total uncertainty. Measurement uncertainty was nearly equivalent in the summer and winter. The contribution of spatial uncertainty due to chamber placement was large in the summer months. During winter, all fluxes were much closer to zero causing the spatial and measurement uncertainties to converge to zero as well. Uncertainty due to the spatial placement of chamber measurements was almost always the highest source of uncertainty in the total methane budget, only being surpassed by super positioned measurement and gap-filling uncertainty in the winter (Fig. 5). Likewise, Xu et al. (2017) found the uncertainty due to Environmental Response Function scaling was the dominant source of error. Spatial uncertainty is further compounded by uncertainty in site level maps, which Forbrich et al. (2011) and Fan et al. (1992) found to be a major limitation to the accuracy of scaling procedures. We surmise that spatial variability of CH_4 fluxes within patch types is one of the greatest hurdles to overcome when scaling chamber measurements (Ambus and Christensen, 1995; Morrissey and Livingston,

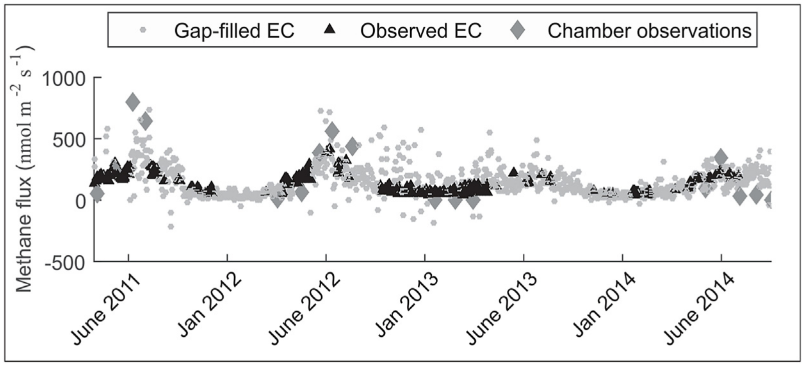

Fig. 4. Fixed-frame CH_4 flux levels and scaled chamber measurements of the permanently flooded wetlands within the park.

1992). This indicates that the full complexity of CH_4 fluxes can only roughly be attributed to land cover types and that local interactions within each patch type may cause large differences in the fluxes. By sampling a large number of points within each patch type in a wetland, we can increase the certainty of the estimated distribution of fluxes within that patch type. As the eddy covariance technique by nature incorporates a broad swath of each patch type, the variability within patch types is considerably less of a problem for this methodology, helping to explain some discrepancies between the two techniques.

The relative error that could be explained due to inaccuracies in the footprint calculation was very small in comparison to spatial and measurement uncertainties (Fig. 5). Uncertainty due to gap-filling (assuming that the observed data is correct) was the lowest of all uncertainty contributions to the final flux signal, increasing our confidence in the explanatory power of the neural network when used to model CH_4 fluxes from wetlands (Dengel et al., 2013; Goodrich et al., 2015; Hatala et al., 2012b; Jammet et al., 2015). All uncertainties are somewhat amplified by natural variations in methane flux due to small differences in both weather and time between samples. We assume these are small effects as the sampling time of the chambers was controlled to be roughly midday in all cases but this may be a cause for further uncertainty in future studies.

Unfortunately, CO_2 fluxes could not undergo the same scaling process used for CH_4 due largely to the inability to conduct chamber measurements of forest trees and thus provide separate estimates

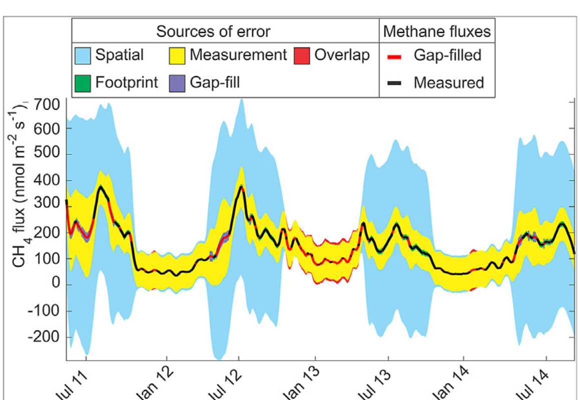

Fig. 5. Corrected flux time series with estimates of uncertainty indicated. By far the greatest uncertainty in summer months was spatial uncertainty. This is related to the intense variability of CH_4 fluxes between two areas with similar terrain cover. In this study, 8 chambers were used for both open water and macrophyte coverage with a total target area of 2 ha between them (the exact breakup of this area into open water and vegetated areas changed annually).

of the CO_2 flux rates of the major CO_2 uptake/emission patches in our wetland site. The mass flux of carbon into the wetland sediments in our site has been measured by Bernal and Mitsch (2013), but did not include carbon storage estimates in forest soils or standing biomass accumulation. Nonetheless, they provided clear evidence that the carbon uptake by the photosynthetic activity of *Typha* spp. plays a large role in the overall GHG budget of that patch type.

4. Conclusions

We developed a method to combine temporally intermittent point measurements (from chambers) for trace gas fluxes with continuous site-level observations (from an EC tower) to determine the fixed-frame time series of CH_4 fluxes in a heterogeneous environment. We determined that fluxes observed by the two methods are statistically similar in magnitude when brought to the same temporal and spatial scale. Adjusting the eddy covariance tower fluxes to the fixed-frame scale of the experimental wetlands made CH_4 measurements from that landscape component more consistent between years.

Using the adjusted eddy covariance fluxes, we were able to quantify the CH_4 budget of the wetland park by land cover. We found that macrophyte vegetation patches in the wetland have the largest contribution to CH_4 fluxes followed by the open water areas. This is most likely because of the soil exudates from the plants during the growing season. The influence of these exudates causes a late summer peak in macrophyte emissions over open water emissions (which are similar to one another for the rest of the year). We also found that the greatest source of uncertainty in quantifying CH_4 emissions from the ORWRP is the heterogeneity of CH_4 emissions within each patch type. This is a strong argument against simply using scaled up point source measurements when estimating site level CH_4 fluxes.

A general strategy can be surmised from these findings for utilizing eddy covariance towers in heterogeneous environments to achieve fixed-frame values. It is of paramount importance to maximize the footprint of the desired patches through careful positioning of the tower, and adjustment to an appropriate height to sample. It may be impossible to obtain a 100% footprint contribution from any particular patch type, as was the case in this study and may be the case in most wetlands that are intrinsically heterogeneous. To compensate for this limitation, the incorporation of chamber measurements and other point measurements of fluxes, such as pore-water dialysis samplers (Pal et al., 2014; Reid et al., 2013), can allow for correction of flux tower observations with a variable footprint to an equivalent fixed-frame CH_4 flux.

Acknowledgements

We thank Lynn McCready, Blanca Bernal, Grace Debbeler, Chas Ellerbrock, William Kenny, Efthalia Chatziefstratiou, Liel Naor-Azrieli, Jorge Villa, Anastasia Sipes, Scott Mesi, and Michele Kingrey for assistance in maintenance and operations of the flux station and the wetland site. The study was funded by NSF CBET grants 1033451 and 1508994, U.S. Geological Survey grant G11AP20099 through the Ohio Water Resources Center projects 2011OH205B and 2012OH259B, and the Ohio Water Development Authority research grants 6835 and 6560. THM was supported in part by NSF Doctoral Dissertation Improvement Grant #1601224 and U.S. Department of Energy's Office of Science Graduate Student Research (SCGSR) Fellowship. THM and ACRS were supported in part through a Fay Fellowship by the Environmental Science Graduate Program. Flux data processing was supported in part by U.S. Department of Energy's Office of Science (AmeriFlux Core Site contract # 7079856).

References

Altor, A.E., Mitsch, W.J., 2006. Methane flux from created riparian marshes: relationship to intermittent versus continuous inundation and emergent macrophytes. Ecol. Eng. 28 (3), 224–234.
Altor, A.E., Mitsch, W.J., 2008. Methane and carbon dioxide dynamics in wetland mesocosms: effects of hydrology and soils. Ecol. Appl. 18 (5), 1307–1320.
Ambus, P., Christensen, S., 1995. Spatial and seasonal nitrous oxide and methane fluxes in Danish forest-, grassland-, and agroecosystems. J. Environ. Qual. 24 (5), 993–1001.
Baldocchi, D.D., Hicks, B.B., Meyers, T.P., 1988. Measuring biosphere-atmosphere exchanges of biologically related gases with micrometeorological methods. Ecology 69 (5), 1331–1340.
Baldocchi, D., Detto, M., Sonnentag, O., Verfaillie, J., Teh, Y.A., Silver, W., Kelly, N.M., 2012. The challenges of measuring methane fluxes and concentrations over a peatland pasture. Agric. Forest Meteorol. 153, 177–187.
Bellisario, L.M., Bubier, J.L., Moore, T.R., Chanton, J.P., 1999. Controls on CH4 emissions from a northern peatland. Glob. Biogeochem. Cycles 13 (1), 81–91.
Bernal, B., Mitsch, W.J., 2013. Carbon sequestration in two created riverine wetlands in the midwestern United States. J. Environ. Qual. 42 (4), 1236–1244.
Blodau, C., Moore, T.R., 2003. Micro-scale CO2 and CH4 dynamics in a peat soil during a water fluctuation and sulfate pulse. Soil Biol. Biochem. 35 (4), 535–547.
Bohn, T.J., Lettenmaier, D.P., Sathulur, K., Bowling, L.C., Podest, E., McDonald, K.C., Friborg, T., 2007. Methane emissions from western Siberian wetlands: heterogeneity and sensitivity to climate change. Environ. Res. Lett. 2 (4).
Bohrer, G., Wolosin, M., Brady, R., Avissar, R., 2007. A Virtual Canopy Generator (V-CaGe) for modeling complex heterogeneous forest canopies at high resolution. Tellus Ser. B-Chem. Phys. Meteorol. 59B (3), 566–576.
Brown, M.G., Humphreys, E.R., Moore, T.R., Roulet, N.T., Lafleur, P.M., 2014. Evidence for a nonmonotonic relationship between ecosystem-scale peatland methane emissions and water table depth. J. Geophys. Res.-Biogeosci. 119 (5), 826–835.
Budishchev, A., Mi, Y., Van Huissteden, J., Belelli-Marchesini, L., Schaepman-Strub, G., Parmentier, F.-J.W., Fratini, G., Gallagher, A., Maximov, T., Dolman, A., 2014. Evaluation of a plot-scale methane emission model using eddy covariance observations and footprint modelling. Biogeosciences 11 (17), 4651–4664.
Christensen, T.R., Ekberg, A., Strom, L., Mastepanov, M., Panikov, N., Oquist, M., Svensson, B.H., Nykanen, H., Martikainen, P.J., Oskarsson, H., 2003. Factors controlling large scale variations in methane emissions from wetlands. Geophys. Res. Lett. 30 (7).
Clement, R.J., Verma, S.B., Verry, E.S., 1995. Relating chamber measurements to eddy-correlation measurements of methane flux. J. Geophys. Res.-Atmos. 100 (D10), 21047–21056.
Dengel, S., Zona, D., Sachs, T., Aurela, M., Jammet, M., Parmentier, F.J.W., Oechel, W., Vesala, T., 2013. Testing the applicability of neural networks as a gap-filling method using CH4 flux data from high latitude wetlands. Biogeosciences 10 (12), 8185–8200.
Desai, A.R., Xu, K., Tian, H., Weishampel, P., Thom, J., Baumann, D., Andrews, A.E., Cook, B.D., King, J.Y., Kolka, R., 2015. Landscape-level terrestrial methane flux observed from a very tall tower. Agric. Forest Meteorol. 201, 61–75.
Detto, M., Montaldo, N., Albertson, J.D., Mancini, M., Katul, G., 2006. Soil moisture and vegetation controls on evapotranspiration in a heterogeneous Mediterranean ecosystem on Sardinia, Italy. Water Resour. Res. 42 (8), W08419.
Detto, M., Verfaillie, J., Anderson, F., Xu, L., Baldocchi, D., 2011. Comparing laser-based open- and closed-path gas analyzers to measure methane fluxes using the eddy covariance method. Agric. Forest Meteorol. 151 (10), 1312–1324.
Fan, S., Wofsy, S.C., Bakwin, P., Jacob, D.J., Anderson, S., Kebabian, P., McManus, J., Kolb, C., Fitzjarrald, D., 1992. Micrometeorological Measurements of CH 4 and CO 2 Exchange Between the Atmosphere and Subarctic Tundra.
Forbrich, I., Kutzbach, L., Wille, C., Becker, T., Wu, J., Wilmking, M., 2011. Cross-evaluation of measurements of peatland methane emissions on microform and ecosystem scales using high-resolution landcover classification and source weight modelling. Agric. Forest Meteorol. 151, 864–874.
Fortuniak, K., Pawlak, W., Bednorz, L., Grygoruk, M., Siedlecki, M., Zieliński, M., 2017. Methane and carbon dioxide fluxes of a temperate mire in Central Europe. Agric. Forest Meteorol. 232, 306–318.
Frasson, R.P.d.M., Bohrer, G., Medvigy, D., Matheny, A.M., Morin, T.H., Vogel, C.S., Gough, C.M., Maurer, K.D., Curtis, P.S., 2015. Modeling forest carbon cycle response to tree mortality: effects of plant functional type and disturbance intensity. J. Geophys. Res.: Biogeosci.
Garrity, S.R., Bohrer, G., Maurer, K.D., Mueller, K.L., Vogel, C.S., Curtis, P.S., 2011. A comparison of multiple phenology data sources for estimating seasonal transitions in forest carbon exchange. Agric. Forest Meteorol. 151, 1741–1752.
Godwin, C.M., McNamara, P.J., Markfort, C.D., 2013. Evening methane emission pulses from a boreal wetland correspond to convective mixing in hollows. J. Geophys. Res.-Biogeosci. 118 (3), 994–1005.
Goodrich, J.P., Campbell, D.I., Roulet, N.T., Clearwater, M.J., Schipper, L.A., 2015. Overriding control of methane flux temporal variability by water table dynamics in a Southern Hemisphere, raised bog. J. Geophys. Res.: Biogeosci. 120 (5), 819–831.
Grosse, W., Armstrong, J., Armstrong, W., 1996. A history of pressurised gas-flow studies in plants. Aquat. Bot. 54 (2-3), 87–100.
Hatala, J.A., Detto, M., Baldocchi, D.D., 2012a. Gross ecosystem photosynthesis causes a diurnal pattern in methane emission from rice. Geophys. Res. Lett. 39 (6), L06409.
Hatala, J.A., Detto, M., Sonnentag, O., Deverel, S.J., Verfaillie, J., Baldocchi, D.D., 2012b. Greenhouse gas (CO2, CH4, H2O) fluxes from drained and flooded agricultural peatlands in the Sacramento-San Joaquin Delta. Agric. Ecosyst. Environ. 150, 1–18.
Hendriks, D., Van Huissteden, J., Dolman, A., 2010. Multi-technique assessment of spatial and temporal variability of methane fluxes in a peat meadow. Agric. Forest Meteorol. 150 (6), 757–774.
Holland, E.A., Robertson, G.P., Greenberg, J., Groffman, Peter M., Boone, Richard D., Gosz, James R., 1999. Soil CO2, N2O, and CH4 exchange. In: Robertson, G.P., Coleman, D.C., Bledsoe, C.S. (Eds.), Standard Soil Methods for Long-term Ecological Research. Oxford University Press, New York, pp. 185–201.
Hommeltenberg, J., Mauder, M., Drösler, M., Heidbach, K., Werle, P., Schmid, H.P., 2014a. Ecosystem scale methane fluxes in a natural temperate bog-pine forest in southern Germany. Agric. Forest Meteorol. 198–199 (0), 273–284.
Hommeltenberg, J., Schmid, H., Drösler, M., Werle, P., 2014b. Can a bog drained for forestry be a stronger carbon sink than a natural bog forest? Biogeosciences 11 (13), 3477–3493.
Hsieh, C.I., Katul, G., Chi, T., 2000. An approximate analytical model for footprint estimation of scaler fluxes in thermally stratified atmospheric flows. Adv. Water Resour. 23 (7), 765–772.
Hutjes, R., Vellinga, O., Gioli, B., Miglietta, F., 2010. Dis-aggregation of airborne flux measurements using footprint analysis. Agric. Forest Meteorol. 150 (7), 966–983.
IPCC (Editor), 2013. Climate Change 2013: The Physical Science Basis. Contribution of Working Group I to the Fifth Assessment Report of the Intergovernmental Panel on Climate Change [Stocker, T.F., Qin, D., Plattner, G.-K., Tignor, M., Allen, S.K., Boschung, J., Nauels, A., Xia, Y., Bex, V., Midgley, P.M. (eds.). IPCC Report. Cambridge University Press Cambridge, United Kingdom and New York, NY, USA, 1535 pp.
Jackowicz-Korczyński, M., Christensen, T.R., Backstränd, K., Crill, P., Friborg, T., Mastepanov, M., Ström, L., 2010. Annual cycle of methane emission from a subarctic peatland. J. Geophys. Res.-Biogeosci. 115.
Jammet, M., Crill, P., Dengel, S., Friborg, T., 2015. Large methane emissions from a subarctic lake during spring thaw: mechanisms and landscape significance. J. Geophys. Res.: Biogeosci. 120 (11), 2289–2305.
Joabsson, A., Christensen, T.R., Wallen, B., 1999. Vascular plant controls on methane emissions from northern peatforming wetlands. Trends Ecol. Evol. 14 (10), 385–388.
Kim, J., Verma, S.B., Billesbach, D.P., 1999. Seasonal variation in methane emission from a temperate Phragmites-dominated marsh: effect of growth stage and plant-mediated transport. Global Change Biol. 5 (4), 433–440.
Kljun, N., Calanca, P., Rotach, M.W., Schmid, H.P., 2015. A simple two-dimensional parameterisation for flux footprint prediction (FFP). Geosci. Model Dev. 8, 3695–3713.
Kutzbach, L., Wagner, D., Pfeiffer, E.M., 2004. Effect of microrelief and vegetation on methane emission from wet polygonal tundra, Lena Delta, Northern Siberia. Biogeochemistry 69 (3), 341–362.
LI-COR, I., 2010. LI-7700 Open Path CH4 Analyzer Instruction Manual.
Lavigne, M., Ryan, M., Anderson, D., Baldocchi, D., Crill, P., Fitzjarrald, D., Goulden, M., Gower, S., Massheder, J., McCaughey, J., 1997. Comparing nocturnal eddy covariance measurements to estimates of ecosystem respiration made by scaling chamber measurements at six coniferous boreal sites. J. Geophys. Res. 102 (D24).
Lee, X., Finnigan, J.J., Paw, T., 2004. Coordinate systems and flux bias error. In: Lee, X., Massman, W., Law, B. (Eds.), Handbook of Micrometeorology, a Guide for Surface Flux Measurement and Analysis. Kluwer Academic Publishers, Dordrecht, the Netherlands, pp. 33–66.

Leppala, M., Oksanen, J., Tuittila, E.S., 2011. Methane flux dynamics during mire succession. Oecologia 165 (2), 489–499.
Li, X., Mitsch, W.J., 2016. Methane emissions from created and restored freshwater and brackish marshes in southwest Florida, USA. Ecol. Eng. 91, 529–536.
Long, K.D., Flanagan, L.B., Cai, T., 2010. Diurnal and seasonal variation in methane emissions in a northern Canadian peatland measured by eddy covariance. Global Change Biol. 16 (9), 2420–2435.
Mack, J.J., Fennessy, M.S., Micacchion, M., Porej, D., 2004. Standardized Monitoring Protocols, Data Analysis and Reporting Requirements for Mitigation Wetlands in Ohio, v. 1.0. Ohio Environmental Protection Agency, Division of Surface Water, Wetland Ecology Group, Columbus, OH.
Massman, W.J., 2000. A simple method for estimating frequency response corrections for eddy covariance systems. Agric. Forest Meteorol. 104 (3), 185–198.
Matthes, J.H., Sturtevant, C., Verfaillie, J., Knox, S., Baldocchi, D., 2014. Parsing the variability in CH4 flux at a spatially heterogeneous wetland: integrating multiple eddy covariance towers with high-resolution flux footprint analysis. J. Geophys. Res.: Biogeosci. 119 (7), 1322–1339.
Maurer, K., Hardiman, B., Vogel, C., Bohrer, G., 2013. Canopy-structure effects on surface roughness parameters: observations in a Great Lakes mixed-deciduous forest. Agric. Forest Meteorol. 177, 24–34.
Metzger, S., Junkermann, W., Mauder, M., Butterbach-Bahl, K., Trancón y Widemann, B., Neidl, F., Schäfer, K., Wieneke, S., Zheng, X., Schmid, H., 2013. Spatially explicit regionalization of airborne flux measurements using environmental response functions. Biogeosciences 10 (4), 2193–2217.
Mikkelä, C., Sundh, I., Svensson, B., Nilsson, M., 1995. Diurnal variation in methane emission in relation to the water table, soil temperature, climate and vegetation cover in a Swedish acid mire. Biogeochemistry 28 (2), 93–114.
Mitsch, W.J., Bernal, B., Nahlik, A.M., Mander, U., Zhang, L., Anderson, C.J., Jorgensen, S.E., Brix, H., 2013. Wetlands, carbon, and climate change. Landscape Ecol. 28 (4), 583–597.
Mitsch, W.J., Zhang, L., Waletzko, E., Bernal, B., 2014. Validation of the ecosystem services of created wetlands: two decades of plant succession, nutrient retention, and carbon sequestration in experimental riverine marshes. Ecol. Eng. 72, 11–24.
Moffat, A.M., Papale, D., Reichstein, M., Hollinger, D.Y., Richardson, A.D., Barr, A.G., Beckstein, C., Braswell, B.H., Churkina, G., Desai, A.R., Falge, E., Gove, J.H., Heimann, M., Hui, D., Jarvis, A.J., Kattge, J., Noormets, A., Stauch, V.J., 2007. Comprehensive comparison of gap-filling techniques for eddy covariance net carbon fluxes. Agric. Forest Meteorol. 147 (3-4), 209–232.
Moore, T.R., Dalva, M., 1993. The influence of temperature and water-table position on carbon-dioxide and methane emissions from laboratory columns of peatland soils. J. Soil Sci. 44 (4), 651–664.
Moore, T.R., De Young, A., Bubier, J.L., Humphreys, E.R., Lafleur, P.M., Roulet, N.T., 2011. A multi-Year record of methane flux at the mer bleue bog, southern Canada. Ecosystems 14 (4), 646–657.
Morin, T.H., Bohrer, G., Frasson, R.P.M., Naor-Azrieli, L., Mesi, S., Stefanik, K., Schäfer, K.V.R., 2014a. Environmental drivers of methane fluxes from an urban temperate wetland park. J. Geophys. Res.: Biogeosci. 119 (11), 2188–2208.
Morin, T.H., Bohrer, G., Naor-Azrieli, L., Mesi, S., Mitsch, W.J., Schäfer, K.V.R., 2014b. The seasonal and diurnal dynamics of methane flux at a created urban wetland. Ecol. Eng. 72, 74–83.
Morrissey, L., Livingston, G., 1992. Methane emissions from Alaska arctic tundra: an assessment of local spatial variability. J. Geophys. Res.: Atmos. 97 (D15), 16661–16670.
Nahlik, A.M., Mitsch, W.J., 2010. Methane Emissions from Created Riverine Wetlands. Wetlands, 30(4): 783–793, with Erratum Published in Wetlands, 31., pp. 449–450 (2011).
Ogunjemiyo, S.O., Kaharabata, S.K., Schuepp, P.H., MacPherson, I.J., Desjardins, R.L., Roberts, D.A., 2003. Methods of estimating CO 2, latent heat and sensible heat fluxes from estimates of land cover fractions in the flux footprint. Agric. Forest Meteorol. 117 (3), 125–144.
Ohkubo, S., Kosugi, Y., Takanashi, S., Mitani, T., Tani, M., 2007. Comparison of the eddy covariance and automated closed chamber methods for evaluating nocturnal CO 2 exchange in a Japanese cypress forest. Agric. Forest Meteorol. 142 (1), 50–65.
Pal, D.S., Reid, M.C., Jaffé, P.R., 2014. Impact of Hurricane Sandy on CH4 released from vegetated and unvegetated wetland microsites. Environ. Sci. Technol. Lett. 1 (9), 372–375.
Papale, D., Valentini, A., 2003. A new assessment of European forests carbon exchanges by eddy fluxes and artificial neural network spatialization. Glob. Change Biol. 9 (4), 525–535.
Parmentier, F., van Huissteden, J., Van Der Molen, M., Schaepman-Strub, G., Karsanaev, S., Maximov, T., Dolman, A., 2011. Spatial and temporal dynamics in eddy covariance observations of methane fluxes at a tundra site in northeastern Siberia. J. Geophys. Res.: Biogeosci. 116 (G3).
Podgrajsek, E., Sahlee, E., Bastviken, D., Holst, J., Lindroth, A., Tranvik, L., Rutgersson, A., 2014. Comparison of floating chamber and eddy covariance measurements of lake greenhouse gas fluxes. Biogeosciences 11 (15), 4225–4233.
Quantum, G., 2013. Development Team, 2012. Quantum GIS Geographic Information System. Open Source Geospatial Foundation Project. Free Software Foundation, India.
Reichstein, M., Falge, E., Baldocchi, D., Papale, D., Aubinet, M., Berbigier, P., Bernhofer, C., Buchmann, N., Gilmanov, T., Granier, A., Grunwald, T., Havrankova, K., Ilvesniemi, H., Janous, D., Knohl, A., Laurila, T., Lohila, A., Loustau, D., Matteucci, G., Meyers, T., Miglietta, F., Ourcival, J.M., Pumpanen, J., Rambal, S., Rotenberg, E., Sanz, M., Tenhunen, J., Seufert, G., Vaccari, F., Vesala, T., Yakir, D., Valentini, R., 2005. On the separation of net ecosystem exchange into assimilation and ecosystem respiration: review and improved algorithm. Global Change Biol. 11 (9), 1424–1439.
Reid, M.C., Tripathee, R., Schäfer, K.V.R., Jaffe, P.R., 2013. Tidal marsh methane dynamics: difference in seasonal lags in emissions driven by storage in vegetated versus unvegetated sediments. J. Geophys. Res.: Biogeosci. 118 (4), 1802–1813.
Rinne, J., Riutta, T., Pihlatie, M., Aurela, M., Haapanala, S., Tuovinen, J.P., Tuittila, E.S., Vesala, T., 2007. Annual cycle of methane emission from a boreal fen measured by the eddy covariance technique. Tellus Ser. B-Chem. Phys. Meteorol. 59 (3), 449–457.
Sachs, T., Wille, C., Boike, J., Kutzbach, L., 2008. Environmental controls on ecosystem-scale CH4 emission from polygonal tundra in the Lena River Delta, Siberia. J. Geophys. Res.- Biogeosci. 113.
Sachs, T., Giebels, M., Boike, J., Kutzbach, L., 2010. Environmental controls on CH4 emission from polygonal tundra on the microsite scale in the Lena river delta, Siberia. Global Change Biol. 16 (11), 3096–3110.
Savage, K.E., Davidson, E.A., 2003. A comparison of manual and automated systems for soil CO2 flux measurements: trade-offs between spatial and temporal resolution. J. Exp. Bot. 54 (384), 891–899.
Schäfer, K., Tripathee, R., Artigas, F., Morin, T., Bohrer, G., 2014. Carbon dioxide fluxes of an urban tidal marsh in the Hudson-Raritan estuary. J. Geophys. Res.: Biogeosci. 119 (11), 2065–2081.
Schrier-Uijl, A.P., Kroon, P.S., Hensen, A., Leffelaar, P.A., Berendse, F., Veenendaal, E.M., 2010. Comparison of chamber and eddy covariance-based CO2 and CH4 emission estimates in a heterogeneous grass ecosystem on peat. Agric. Forest Meteorol. 150 (6), 825–831.
Sha, C., Mitsch, W.J., Mander, U., Lu, J.J., Batson, J., Zhang, L., He, W.S., 2011. Methane emissions from freshwater riverine wetlands. Ecol. Eng. 37 (1), 16–24.
Stefanik, K.C., Mitsch, W.J., 2014. Metabolism and methane flux of dominant macrophyte communities in created riverine wetlands using open system flow through chambers. Ecol. Eng. 72, 67–73.
Ström, L., Mastepanov, M., Christensen, T.R., 2005. Species-specific effects of vascular plants on carbon turnover and methane emissions from wetlands. Biogeochemistry 75 (1), 65–82.
Sturtevant, C.S., Oechel, W.C., 2013. Spatial variation in landscape-level CO2 and CH4 fluxes from arctic coastal tundra: influence from vegetation, wetness, and the thaw lake cycle. Global Change Biol. 19 (9), 2853–2866.
Terazawa, K., Ishizuka, S., Sakata, T., Yamada, K., Takahashi, M., 2007. Methane emissions from stems of Fraxinus mandshurica var. japonica trees in a floodplain forest. Soil Biol. Biochem. 39 (10), 2689–2692.
US-EPA, 2012. Memorandum of Agreement Between the Department of the Army and the Environmental Protection Agency. Environmental Protection Agency.
Waletzko, E.J., Mitsch, W.J., 2013. The carbon balance of two riverine wetlands fifteen years after their creation. Wetlands.
Waletzko, E.J., Mitsch, W.J., 2014. Methane emissions from wetlands: an in situ side-by-side comparison of two static accumulation chamber designs. Ecol. Eng. 72, 95–102.
Wang, W., Davis, K.J., Cook, B.D., Butler, M.P., Ricciuto, D.M., 2006. Decomposing CO2 fluxes measured over a mixed ecosystem at a tall tower and extending to a region: a case study. J. Geophys. Res.: Biogeosci. 111 (G2).
Wang, J.M., Murphy, J.G., Geddes, J.A., Winsborough, C.L., Basiliko, N., Thomas, S.C., 2013. Methane fluxes measured by eddy covariance and static chamber techniques at a temperate forest in central Ontario, Canada. Biogeosciences 10 (6), 4371–4382.
Webb, E.K., Pearman, G.I., Leuning, R., 1980. Correction of flux measurements for density effect due to heat and water vapour transfer. Q. J. R. Meteorolog. Soc. 106 (447), 85–100.
Whiting, G.J., Chanton, J.P., 1993. Primary production control of methane emission from wetlands. Nature 364 (6440), 794–795.
Whiting, G.J., Chanton, J.P., 1996. Control of the diurnal pattern of methane emission from emergent aquatic macrophytes by gas transport mechanisms. Aquat. Bot. 54 (2-3), 237–253.
Wille, C., Kutzbach, L., Sachs, T., Wagner, D., Pfeiffer, E.M., 2008. Methane emission from Siberian arctic polygonal tundra: eddy covariance measurements and modeling. Glob. Change Biol. 14 (6), 1395–1408.
Wilson, J.O., Crill, P.M., Bartlett, K.B., Sebacher, D.I., Harriss, R.C., Sass, R.L., 1989. Seasonal-variation of methane emissions from a temperate swamp. Biogeochemistry 8 (1), 55–71.
Xu, K., Metzger, S., Desai, A.R., 2017. Upscaling tower-observed turbulent exchange at fine spatio-temporal resolution using environmental response functions. Agric. Forest Meteorol. 232, 10–22.
Yu, L.F., Wang, H., Wang, G.S., Song, W.M., Huang, Y., Li, S.G., Liang, N.S., Tang, Y.H., He, J.S., 2013. A comparison of methane emission measurements using eddy covariance and manual and automated chamber-based techniques in Tibetan Plateau alpine wetland. Environ. Pollut. 181, 81–90.
Zhang, Y., Sachs, T., Li, C.S., Boike, J., 2012. Upscaling methane fluxes from closed chambers to eddy covariance based on a permafrost biogeochemistry integrated model. Glob. Change Biol. 18 (4), 1428–1440.
von Fischer, J.C., Rhew, R.C., Ames, G.M., Fosdick, B.K., von Fischer, P.E., 2010. Vegetation height and other controls of spatial variability in methane emissions from the Arctic coastal tundra at Barrow, Alaska. J. Geophys. Res.: Biogeosci. 115 (G4).